Evidence for northward expansion of Antarctic Bottom Water mass in the Southern Ocean during the last glacial inception

Aline Govin, Elisabeth Michel, Laurent Labeyrie, Claire Waelbroeck, Fabien L Dewilde, Eystein Jansen

PALEOCEANOGRAPHY, VOL. 24, PA1202, doi:10.1029/2008PA001603, 2009

Evidence for northward expansion of Antarctic Bottom Water mass in the Southern Ocean during the last glacial inception

Aline Govin,[1,2] Elisabeth Michel,[1] Laurent Labeyrie,[1] Claire Waelbroeck,[1] Fabien Dewilde,[1] and Eystein Jansen[3]

Received 31 January 2008; revised 12 October 2008; accepted 22 October 2008; published 22 January 2009.

[1] We investigated deep water changes in the Southern Ocean during the last glacial inception, in relationship to surface hydrology and global climatology, to better understand the mechanisms of the establishment of a glacial ocean circulation. Changes in benthic foraminiferal $\delta^{13}C$ from three high-resolution cores are compared and indicate decoupled intermediate and deep water changes in the Southern Ocean. From the comparison with records from the North Atlantic, South Atlantic, and the Southern Ocean, we show that the early southern deep water $\delta^{13}C$ drop observed at the MIS 5.5–5.4 transition occurred before any significant reduction of North Atlantic Deep Water ventilation. We propose that this drop is linked to the northward expansion of poorly ventilated Antarctic Bottom Water (AABW) mass in the Southern Ocean. Associated with an early cooling in the high southern latitudes, the westerly winds and surface oceanic fronts would migrate equatorward, thus weakening the upwelling of Circumpolar Deep Waters. Reduced heat brought to Antarctic surface waters would enhance sea ice formation during winters and the deep convection of cold and poorly ventilated AABW.

Citation: Govin, A., E. Michel, L. Labeyrie, C. Waelbroeck, F. Dewilde, and E. Jansen (2009), Evidence for northward expansion of Antarctic Bottom Water mass in the Southern Ocean during the last glacial inception, *Paleoceanography*, *24*, PA1202, doi:10.1029/2008PA001603.

1. Introduction

[2] The glacial oceanic circulation was significantly different from the modern one. Past reconstructions of the carbon isotope composition ($\delta^{13}C$) of dissolved inorganic carbon for the Last Glacial Maximum showed an increased intermediate-deep waters $\delta^{13}C$ gradient in the Atlantic Ocean [*Curry et al.*, 1988; *Duplessy et al.*, 1988]. The well-ventilated North Atlantic Deep Waters (NADW) sank to shallower depths during glacial times, forming the water mass called Glacial North Atlantic Intermediate Waters (GNAIW) [*Duplessy et al.*, 1988], whereas poorly ventilated Antarctic Bottom Waters (AABW) filled the deep glacial Atlantic below GNAIW. A similar ventilation pattern is observed in the South Atlantic during glacial times, with well-ventilated intermediate waters (high $\delta^{13}C$ values) overlying poorly ventilated deep waters (low $\delta^{13}C$ values) [*Hodell et al.*, 2003; *Mackensen et al.*, 2001].

[3] However, little is known on the establishment of such a glacial thermohaline circulation pattern at the initiation of the last glacial period. Most past reconstructions in the North Atlantic Ocean and the Nordic Seas show an early surface cooling in the high northern latitudes, prior to Northern Hemisphere ice sheets growth [*Cortijo et al.*, 1994; *McManus et al.*, 1994], followed by a shoaling of North Atlantic Deep Waters [*Adkins et al.*, 1997; *Evans et al.*, 2007]. Although high-resolution records are now available in the Southern Ocean for the last glacial cycle [*Hodell et al.*, 2003; *Molyneux et al.*, 2007; *Pahnke and Zahn*, 2005], so far no detailed work investigated the precise role and timing of the changes in Southern Ocean circulation during the last glacial inception.

[4] Different mechanisms have been proposed, associated with a rapid switch from Northern Component Waters to Southern Component Waters at middepths in the South Atlantic [*Molyneux et al.*, 2007], or emphasizing the key role of the subtropical front as amplifier and vehicle for the transfer of climatic change to the Southern Ocean [*Cortese et al.*, 2007]. But published data are insufficient to give the necessary integrated view of the Southern Ocean circulation changes and associated mechanisms during the last glacial inception. This study aims at better constraining the deep water circulation changes in the Southern Ocean over the period 130–60 ka, period of inception of the last glacial ice sheets, in relationship to surface hydrology and global climatology. The analysis was done in two steps. First, planktic and benthic foraminiferal records of three high-resolution Southern Ocean cores were compared to build a reference frame for deep and intermediate water changes over the period. In a second step, these records were compared to three published North and South Atlantic records to precise changes in NADW ventilation, and to four lower-

[1] LSCE, IPSL, CEA, UVSQ, CNRS, Gif sur Yvette, France.
[2] Also at Bjerknes Centre for Climate Research, University of Bergen, Bergen, Norway.
[3] Bjerknes Centre for Climate Research, University of Bergen, Bergen, Norway.

0883-8305/09/2008PA001603$12.00

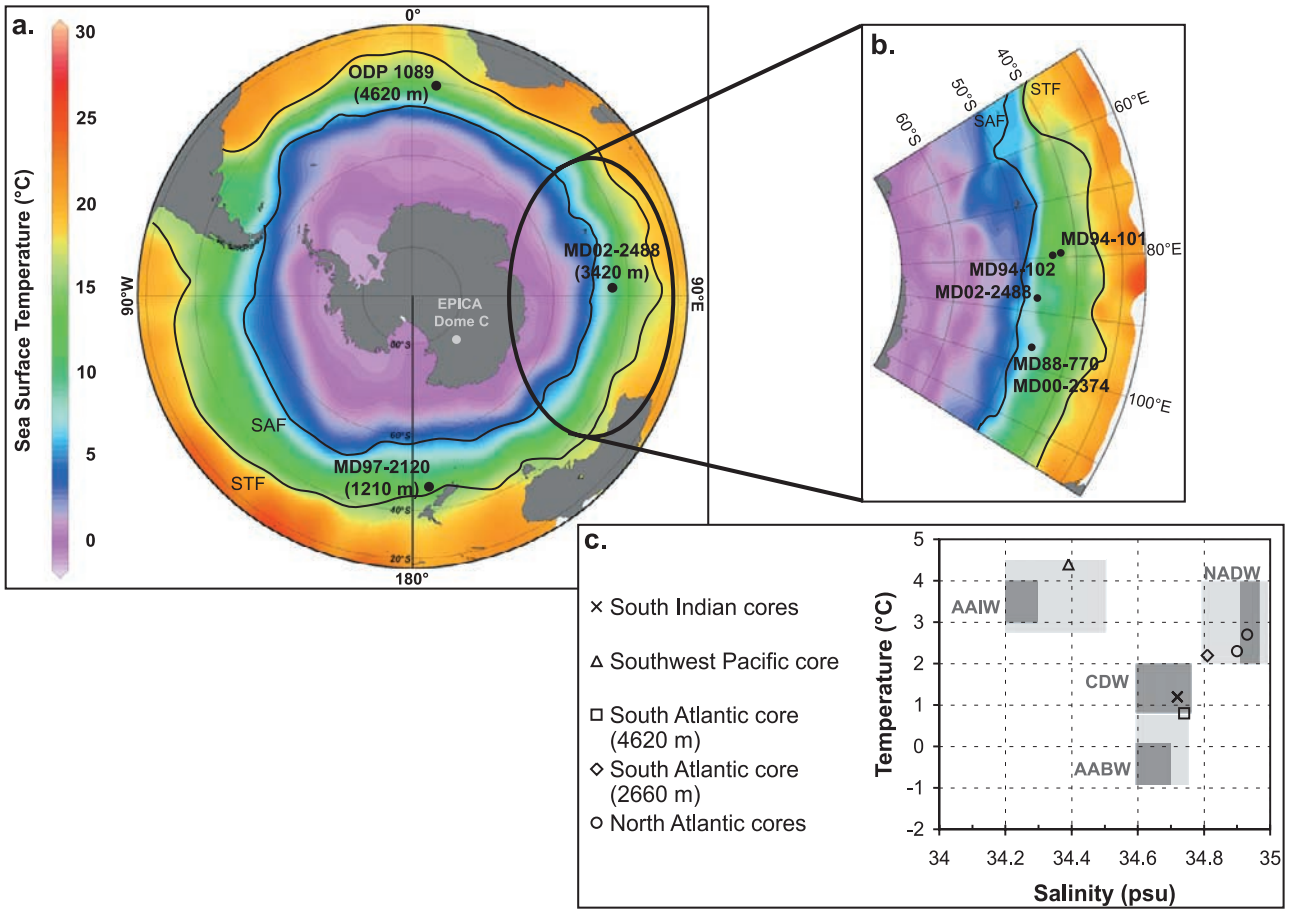

Figure 1. (a) Map of sea surface temperature (SST) [*Olbers et al.*, 1992] in the Southern Ocean. (b) Zoom on the Indian sector of the Southern Ocean. These maps have been created using the Ocean Data View program (R. Schlitzer, Ocean Data View, 2006, Alfred Wegener Institute for Polar and Marine Research, Bremerhaven, Germany, available at http://odv.awi.de). (c) Temperature-salinity diagram: the characteristics of the main water masses are defined senso stricto (i.e., source areas characteristics) by the dark gray-shaded areas and senso largo (i.e., from the commonly used definition of these water masses) by the light gray-shaded areas. The characteristics of each core considered here (Table 1) are represented by the symbols. It shows that the North Atlantic (open circles) and South Atlantic (open diamond) cores are bathed by North Atlantic Deep Waters (NADW), the southwestern Pacific core MD97-2120 (open triangle) is bathed by Antarctic Intermediate Waters (AAIW), all South Indian cores (crosses) are bathed by Circumpolar Deep Waters (CDW), and the South Atlantic ODP 1089 site (open square) is also bathed by Lower CDW, with a stronger influence of Antarctic Bottom Waters (AABW).

resolution records, forming a meridional transect in the Indian sector of the Southern Ocean.

2. Material and Methods

2.1. Study Sites

[5] The water depths and locations of the cores considered in this work are reported in Table 1. The evolution of intermediate and deep waters in the Southern Ocean is reconstructed using a new high-resolution record from the South Indian Ocean, core MD02-2488 (southern flank of the South Indian ridge, 3420 m) lying in Circumpolar Deep Waters (CDW), compared with two published records, the first from the southwest Pacific, currently bathed in Antarctic Intermediate water (AAIW) (core MD97-2120, Chatham Rise, 1210 m water depth) [*Pahnke and Zahn*, 2005; *Pahnke et al.*, 2003], and the second from the South Atlantic, bathed by Lower CDW (ODP 1089, Cape Basin, 4620 m) [*Mortyn et al.*, 2003; *Ninnemann*, 1999] (Figures 1a and 1c). The newly published core MD02-2488 is characterized by a relatively high sedimentation rate (15 cm/ka in average): it was collected on a seamount on the southern flank of the Indian ridge, protected from the Antarctic circumpolar current [*Dezileau et al.*, 2000; *Mazaud et al.*, 2007].

[6] The three Southern Ocean cores are all located between the subantarctic and the subtropical fronts, i.e., in the subantarctic zone of the Southern Ocean (Figure 1a). Because of the mostly zonal organization of the Southern Ocean [*Schmitz*, 1996], we assume that past surface hydrology

Table 1. Location and Characteristics of the Sites Considered in This Study

Core	Latitude	Longitude	Depth (m)	SST[a] (°C)	T_{dw}[b] (°C)	$\delta^{18}O_{dw}$[b] (‰ SMOW)	S_{dw}[b] (psu)	References[c]
MD02-2488	46°28.8'S	88°01.3'E	3420	9.1	1.2	−0.01	34.72	1
MD97-2120	45°32.1'S	174°55.9'E	1210	13.5	4.4	0.01	34.39	2
ODP 1089	40°56.2'S	9°53.7'E	4621	12.2	0.8	−0.11	34.74	3
MD94-101	42°30'S	79°25'E	2920	13.0	1.2	−0.01	34.72	4
MD94-102	43°30.3'S	79°50.2'E	3205	12.0	1.2	−0.01	34.72	4
MD00-2374	46°02'S	96°29'E	3250	8.1	1.2	−0.01	34.72	5
MD88-770	46°01'S	96°27'E	3290	8.1	1.2	−0.01	34.72	6
SU90-08	43°03.1'N	30°02.5'W	3080	20.5	2.7	0.24	34.93	7
CH69-K09	41°45.4'N	47°21'W	4100	20.4	2.3	0.24	34.90	8
MD02-2589	41°26.03'S	25°15.30'E	2660	16.4	2.2	−0.04	34.81	9

[a]Modern summer sea surface temperature (SST) data are from [*Levitus and Boyer*, 1994].
[b]Modern deep water temperature (T_{dw}) and $\delta^{18}O$ ($\delta^{18}O_{dw}$) are from the GISS database [*Schmidt et al.*, 1999]: WOCE11 data [*Meredith et al.*, 1999] for ODP 1089, NODC ID:35-9439 CIVA2 campaign for core MD02-2589, and GEOSECS data [*Ostlund et al.*, 1987] for all other cores.
[c]References are as follows: 1, this study; 2, *Pahnke and Zahn* [2005] and *Pahnke et al.* [2003]; 3, *Mortyn et al.* [2003] and *Ninnemann* [1999]; 4, *Lemoine* [1998] and *Salvignac* [1998]; 5, *Duplessy et al.* [2007]; 6, *Labeyrie et al.* [1996]; 7, *Cortijo* [1995] and *Grousset et al.* [1993]; 8, *Cortijo* [1995] and *Labeyrie et al.* [1999]; 9, *Molyneux et al.* [2007].

evolved similarly in the subantarctic zone of the different oceanic basins [*Barrows et al.*, 2007].

[7] Four additional low-resolution cores from the Indian sector of the Southern Ocean were collected close to MD02-2488 site, along a north-south transect (42.5–46.5°S) (Table 1). They cover the entire subantarctic zone, from the subtropical front (cores MD94-101 and MD94-102) to the subantarctic front (cores MD88-770 and MD00-2374) (Figure 1b). Collected at similar water depths (around 3200 m), the sites are all presently bathed by the same water mass, Circumpolar Deep Waters.

[8] To illustrate deep water changes in the North and South Atlantic, we used the published isotopic records from two cores (Table 1): SU90-08 (3080 m) [*Cortijo*, 1995; *Grousset et al.*, 1993] and CH69-K09 (4100 m) [*Cortijo*, 1995; *Labeyrie et al.*, 1999] from the western side of the North Atlantic, and core MD02-2589 (2660 m) [*Molyneux et al.*, 2007] from the South Atlantic. All cores presently lie in North Atlantic Deep Waters (NADW).

2.2. Methods

2.2.1. Isotopic Analyses

[9] Hydrological properties of surface and deep waters are derived from the oxygen and carbon isotopic composition of planktic and benthic foraminifera, respectively. The $^{18}O/^{16}O$ ratio ($\delta^{18}O$, expressed in ‰ versus PDB) is a function of both seawater temperature and $\delta^{18}O$, which in turn depends on global ice volume changes and local hydrological (salinity) variations [*Shackleton*, 1974].

[10] The $^{13}C/^{12}C$ ratio ($\delta^{13}C$, expressed in ‰ versus PDB) of the epifaunal benthic species *Cibicides* reflects the $\delta^{13}C$ of dissolved inorganic carbon (ΣCO_2) in seawater, and is used as a tracer of deep water ventilation [*Curry et al.*, 1988; *Duplessy et al.*, 1988; *Labeyrie and Duplessy*, 1985]. Primarily controlled by the biological cycling of ^{13}C depleted organic matter [*Kroopnick*, 1985], the $\delta^{13}C$ of seawater ΣCO_2 is also affected by air-sea CO_2 exchanges [*Lynch-Stieglitz et al.*, 1995]. On an interglacial-glacial time scale, it integrates mean global ocean $\delta^{13}C$ changes linked to the degradation of ^{13}C-depleted continental vegetation and its transfer to the ocean (or reciprocally, increase in biospheric carbon reservoirs) [*Shackleton*, 1977]. Finally, although *Mackensen et al.* [1993] proposed that a "phytodetritus effect" could affect the *Cibicides* $\delta^{13}C$ values in highly productive zones of the Southern Ocean, *Mackensen et al.* [2001] showed that this effect was limited and did not explain the lowest $\delta^{13}C$ signal recorded in the Southern Ocean during the Last Glacial Maximum.

[11] The foraminiferal $\delta^{18}O$ and $\delta^{13}C$ of the newly published core MD02-2488 have been measured at LSCE on Finnigan MAT251 and Finnigan Δ+ mass spectrometers. Isotopic data of the South Indian cores MD94-101 and MD94-102 (Table 1) have also been measured on the MAT251 mass spectrometer in Gif sur Yvette [*Lemoine*, 1998]; the isotopic records of all other cores have been published previously (Table 1). VPDB (Vienna PDB) is defined with respect to NBS 19 calcite standard ($\delta^{18}O$ = −2.20‰ and $\delta^{13}C$ = +1.95‰). The MAT251 mass spectrometer from LSCE presents source memory effects; a correction by the double standards method is applied to all measurements (derived from *Ostermann and Curry* [2000]). The Finnigan Δ+ mass spectrometer does not need that correction. The mean external reproducibility (1σ) of carbonate standards is ±0.05‰ for $\delta^{18}O$ and ±0.03‰ for $\delta^{13}C$. The mean external reproducibility (1σ) of foraminifera (i.e., pooled standard deviation calculated from the benthic and planktic values of 23 and 22 replicated levels, respectively) is estimated at ±0.09‰ for $\delta^{18}O$ and ±0.16‰ for $\delta^{13}C$ for benthic foraminifera, and at ±0.16‰ for $\delta^{18}O$ and ±0.22‰ for $\delta^{13}C$ for planktic foraminifera.

[12] Planktic (*Globigerina bulloides*) and benthic (*Cibicides kullenbergi*) foraminifera from core MD02-2488 were picked in the 250–315 μm and > 150 μm fractions, respectively. The samples were cleaned in a methanol ultrasonic bath during a few seconds then roasted under vacuum at 380°C for 45 min, prior to isotopic analyses [*Duplessy*, 1978]. High-resolution measurements (each 2 cm, i.e., roughly each 0.2 ka) were performed during MIS 5.5 and the MIS 5.5–5.4 and 5.1–4 transitions, whereas the remainder of MIS 5 (stages 5.4 to 5.1) was analyzed at a lower resolution (each 10 cm, i.e., around each 1 ka). The planktic $\delta^{18}O$ record obtained on core MD02-2488 is shown over the last glacial cycle in Figure 2: marine isotope stage 5

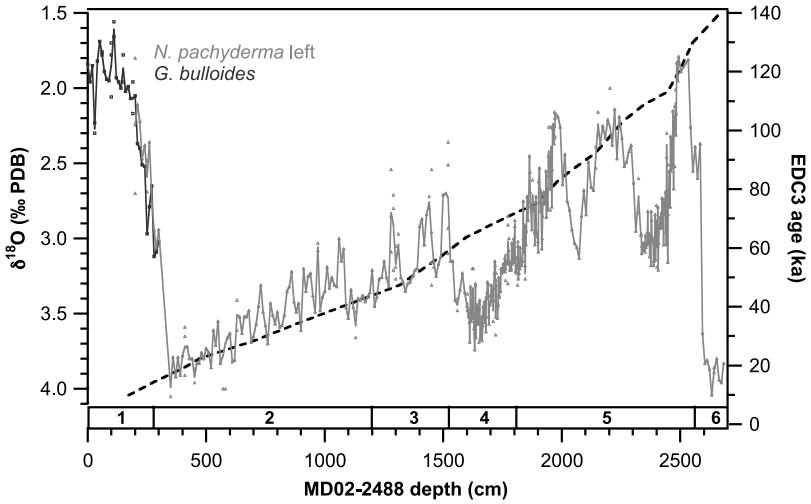

Figure 2. Planktic $\delta^{18}O$ record from core MD02-2488 (measured on *Globigerina bulloides* (dark gray) for the first 300 cm and on *Neogloboquadrina pachyderma* left (light gray) elsewhere) as a function of depth, over the last climatic cycle. The age-depth relationship defined in this core is shown (black dashed line). Symbols represent replicates. Marine isotope stages are shown at the bottom.

presents a particularly high sedimentation rate, with about 10 m of sediment for that period.

2.2.2. Sea Surface Temperature Reconstructions

[13] The sea surface temperature (SST) reconstruction for core MD02-2488 is derived from a linear regression (R^2 = 0.72) between the abundance of the subpolar planktic foraminifera species, *Neogloboquadrina pachyderma* sinistral and the summer SST, calculated using a database of 245 core tops from the Southern Ocean [*Kucera et al.*, 2005] over a temperature range of 3 to 11°C (i.e., percentage of *N. pachyderma* sinistral > 6%) (Figure 3). The uncertainty of the SST reconstruction is ±1.7°C (1σ). This relationship was used to reconstruct a low-resolution (∼1 ka) SST record over MIS 6 to 3 (Figure 4).

[14] During the warm part of MIS 5.5, the abundance of *N. pachyderma* sinistral is however too low (<6%) in core

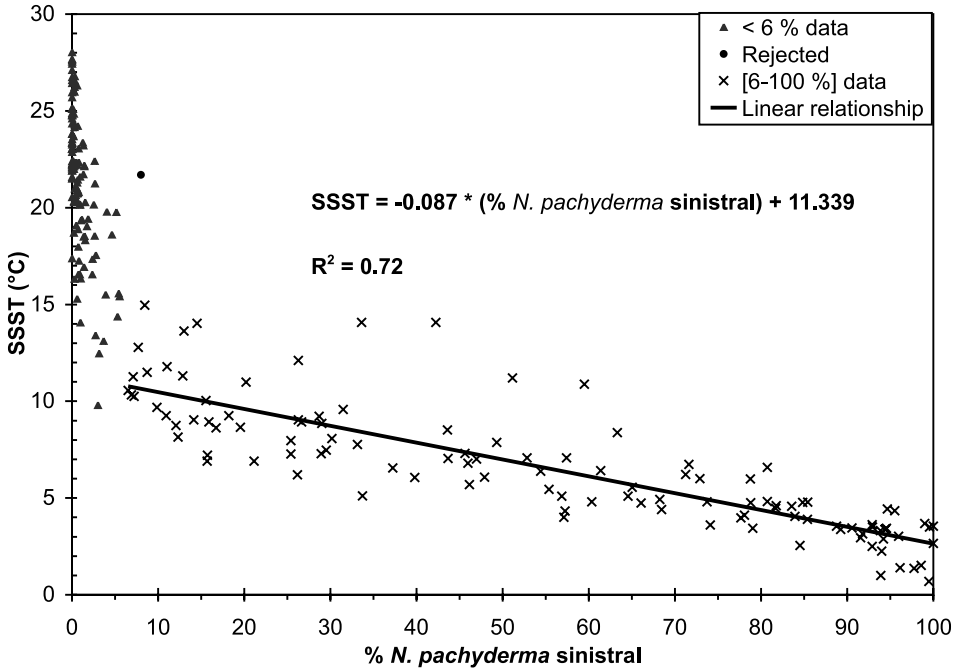

Figure 3. Linear relationship defined between the percentage of *N. pachyderma* sinistral and the summer sea surface temperature (SSST), valid over a 3–11°C temperature range, in the Southern Ocean (database of 245 core tops) [*Kucera et al.*, 2005].

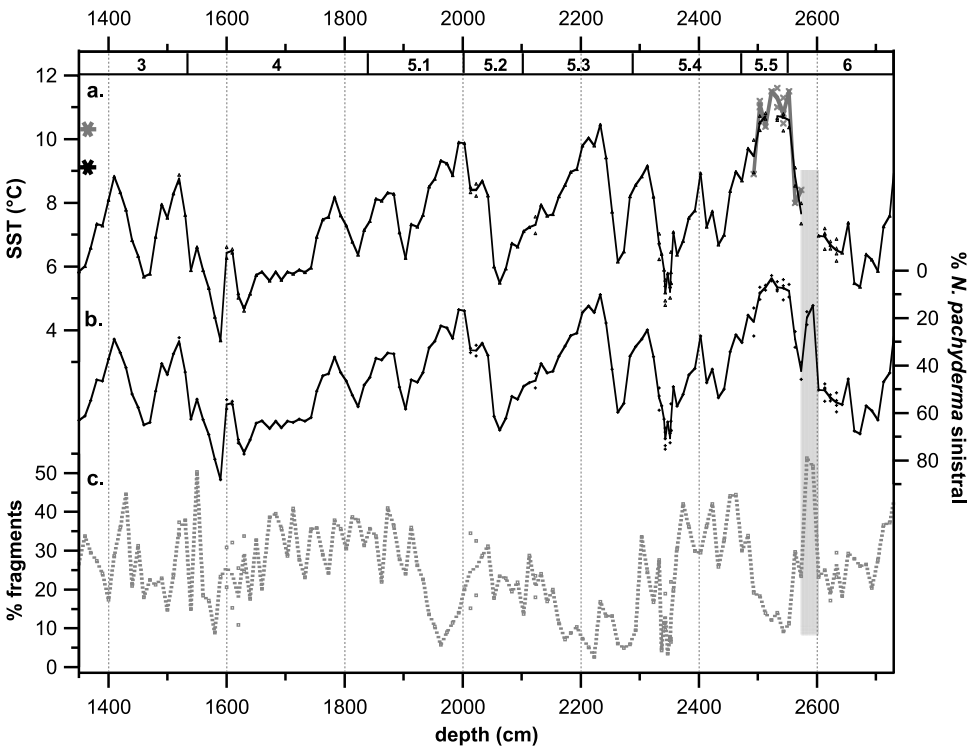

Figure 4. Sea surface temperature reconstruction in the Southern Ocean core MD02-2488, as a function of depth. (a) SST calculated from the percentage of the polar species *N. pachyderma* sinistral (black curve) and from the planktic foraminiferal assemblages (thick gray curve). (b) Percentage of *N. pachyderma* sinistral (black curve). (c) Percentage of fragments, a dissolution proxy (gray dotted line). Symbols indicate replicates. The black star along the SST *y* axis indicates the modern summer SST at MD02-2488 site (9.1°C) [*Levitus and Boyer*, 1994], whereas the gray star represents the temperature reconstructed at the core top (10.3°C), averaged for both methods. The gray-shaded area highlights the dissolution peak of Termination II, where no SST can be reconstructed. Isotopic stages are reported at the top.

MD02-2488 to allow a quantitative SST reconstruction: full foraminiferal assemblages were therefore counted over that period (Figure 4). Summer sea surface temperatures were calculated by the Modern Analog Technique (keeping the five best analogs) [*Prell*, 1985], using the Southern Ocean database [*Kucera et al.*, 2005] and the PaleoAnalogs software [*Theron et al.*, 2004]. The uncertainty of the summer SST reconstruction is estimated to be ±1.4°C (1σ) in the South Atlantic with the MAT method [*Kucera et al.*, 2005].

[15] Both methods (for percentage of *N. pachyderma* sinistral > 6%) give similar temperature results, within uncertainties (Figure 4). The Early Holocene (core top) summer SST at core MD02-2488 site, estimated to be 10.4°C (from the percentage of *N. pachyderma* sinistral only) or 10.2°C (from full foraminiferal assemblages), is, within the uncertainties, similar to the observed summer SST at the site (Table 1). Besides, a peak of particularly low percentages of *N. pachyderma* sinistral is observed during Termination II (Figure 4, gray-shaded area). It is associated with a period of high dissolution, as indicated by high percentages of fragments (>50%) (Figure 4c) and by the relative increase in the proportion of a more robust planktic species *Globigerinoides inflata* (not shown): the SST reconstruction based on assemblages of foraminifera is not reliable in core MD02-2488 during this interval.

[16] We used for core MD97-2120, the Mg/Ca-based SST reconstruction of *Pahnke et al.* [2003], and for cores MD94-101 and MD94-102, the available Modern Analogue Technique SST reconstructions (based on full foraminiferal assemblages) of *Salvignac* [1998]. For core MD88-770, we recalculated the summer SST of *Labeyrie et al.* [1996] on the basis of the full foraminiferal assemblages using the Modern Analogue Technique [*Prell*, 1985]. No SST reconstruction based on foraminifera is unfortunately available for ODP site 1089, because of a high dissolution at that site [*Hodell et al.*, 2003].

2.3. Age Model

[17] The construction of a common chronostratigraphy for all Southern Ocean high-resolution cores is critical for our study. A direct correlation between benthic δ^{18}O records is commonly applied. However, the δ^{18}O of benthic foraminifera not only reflects global ice volume variations, but is also affected by deep water δ^{18}O and temperature changes [*Labeyrie et al.*, 1987; *Skinner and Shackleton*, 2003]. Because possible leads and lags between hydrological changes in intermediate and deep water are of interest for our study, we adopted another approach.

[18] On the basis of the hypothesis that surface water changes are simultaneous over the subantarctic zone of the

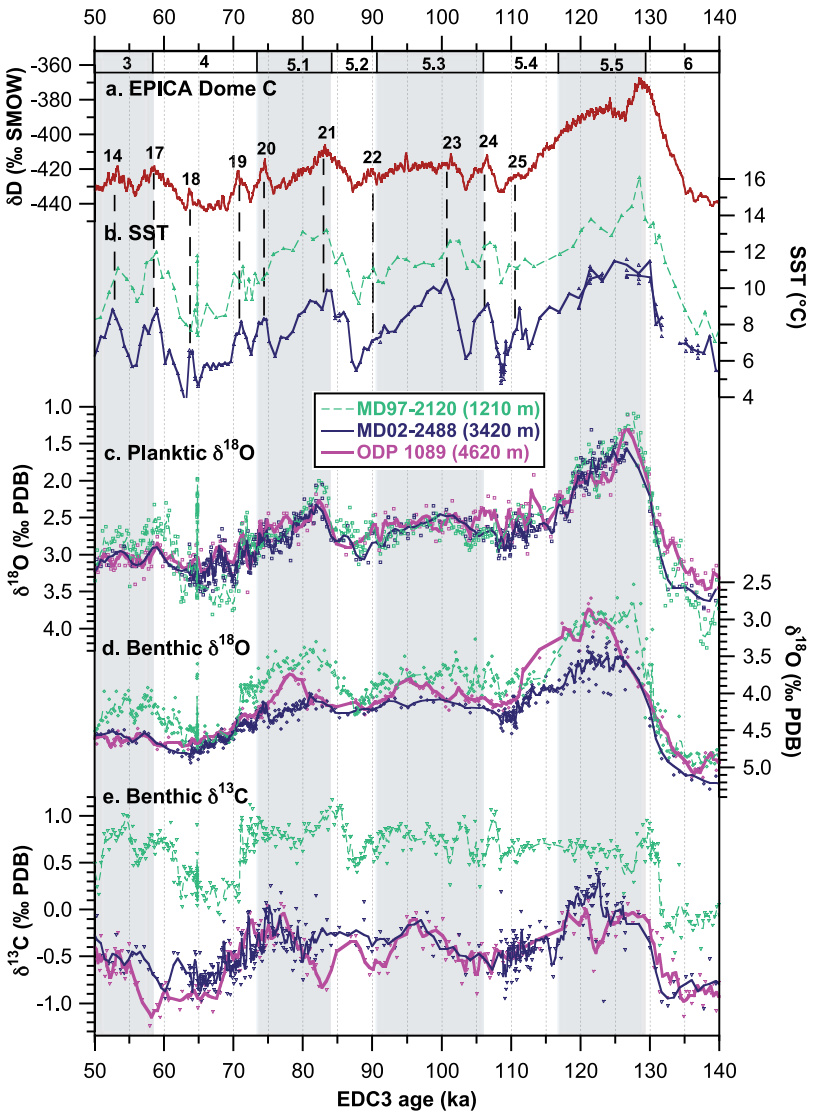

Figure 5. (a) EPICA Dome C deuterium record (dark red curve). Comparison of (b) sea surface temperature, (c) planktic (*G. bulloides*) $\delta^{18}O$, (d) benthic $\delta^{18}O$, and (e) benthic $\delta^{13}C$ data of cores MD97-2120 (1210 m, dashed green curve) [*Pahnke and Zahn*, 2005; *Pahnke et al.*, 2003], MD02-2488 (3420 m, plain dark blue curve) (this study), and ODP site 1089 (4620 m, thick pink curve) [*Mortyn et al.*, 2003; *Ninnemann*, 1999] on the common time scale. The numbers refer to the Antarctic Isotope Maximums [*EPICA Community Members*, 2006]. The symbols represent all data, and the curves represent a three-point moving average. The marine isotope stages are indicated at the top, with the warm substages highlighted by the gray-shaded areas.

Southern Ocean [*Barrows et al.*, 2007; *Cortese et al.*, 2007], we synchronized the planktic $\delta^{18}O$ and SST records of cores MD97-2120 and ODP 1089 to those of core MD02-2488 (Figure 5). SST and planktic $\delta^{18}O$ records indeed show similar values and variations over the period 140–50 ka (Figures 5b and 5c), supporting our assumption. Although not directly tied, the benthic $\delta^{18}O$ records remain globally consistent between the different cores (Figure 5d), with only one major difference: the low $\delta^{18}O$ peaks from ODP site 1089 lag the minimum $\delta^{18}O$ values from cores MD02-2488 and MD97-2120 during the warm marine isotope substages 5.5, 5.3 and 5.1 (Figure 5d). MIS 5.5–5.4 transition in the ODP 1089 benthic data is however poorly constrained, by only two points.

[19] We then derived a chronology based on the assumption that the major temperature changes occur simultaneously in the subantarctic surface waters and in the atmosphere above inland Antarctica [*Sowers et al.*, 1993; *Waelbroeck et al.*, 1995]. Indeed, most of the Antarctic Isotope Maximums (AIM) [*EPICA Community Members*, 2006] recorded in EPICA Dome C (Figure 5a) have a clear temperature signature in the subantarctic surface waters [*Pahnke et al.*, 2003] (Figure 5b). Therefore, we tied the SST records of both cores MD97-2120 [*Pahnke et al.*, 2003] and MD02-2488 (this

Table 2. Amplitude and Standard Deviation (σ) of SST, Planktic (*G. bulloides*) δ^{18}O, Benthic δ^{18}O, and δ^{13}C Changes During the MIS 5.5–5.4 and MIS 5.1–4 Transitions

Core	SST (°C): Difference ($\pm\sigma$)	Planktic δ^{18}O (‰ PDB)		Benthic δ^{18}O[d] (‰ PDB)		Benthic δ^{13}C (‰ PDB): Difference ($\pm\sigma$)
		Difference ($\pm\sigma$)	Ice Volume Corrected[e,f]	Difference ($\pm\sigma$)	Ice Volume Corrected[e,f]	
			MIS 5.5–5.4 Transition[a]			
MD97-2120	−2.7 ± 1.4	0.99 ± 0.30	0.59, i.e., −2.6°C	0.90 ± 0.18	0.50, i.e., −2.2°C	0.05 ± 0.19
MD02-2488	−4.1 ± 1.2	1.02 ± 0.23	0.62, i.e., −2.7°C[g]	0.72 ± 0.24	0.32, i.e., −1.4°C	−0.54 ± 0.34
ODP 1089	none[b]	0.67 ± 0.32	0.27, i.e., −1.2°C	1.05 ± 0.20	0.65, i.e., −2.8°C	−0.37 ± 0.12
			MIS 5.1–4 Transition[a]			
MD97-2120[c]	−4.1 ± 0.9	0.91 ± 0.34	0.43, i.e., −1.9°C[g]	0.98 ± 0.18	0.50, i.e., −2.2°C	−0.53 ± 0.19
MD02-2488	−3.6 ± 1.1	0.78 ± 0.25	0.30, i.e., −1.3°C[g]	0.63 ± 0.11	0.15, i.e., −0.7°C	−0.44 ± 0.23
ODP 1089	none[b]	0.63 ± 0.29	0.15, i.e., −0.7°C	0.61 ± 0.18	0.13, i.e., −0.6°C	−0.70 ± 0.18

[a]The means and standard deviations were calculated over the intervals 126–120 ka for MIS 5.5, 111–107.5 ka for MIS 5.4, 85–79 ka for MIS 5.1, and 67–62 ka for MIS 4 for each proxy, except for benthic δ^{13}C data during MIS 5.1, where we considered a late MIS 5.1 (78.5–72 ka).

[b]No SST record based on formaninifera is available for ODP 1089.

[c]The anomalous values of MD97-2120 during MIS 4 (considered as due to sedimentological perturbation) are not considered here.

[d]The Cibicides δ^{18}O values have been adjusted by +0.64‰ to bring them to the *Uvigerina* scale [*Shackleton*, 1974]. Isotopic data of ODP site 1089 [*Hodell et al.*, 2002] have been multiplied by 1.048 to fit the values of ODP 1089 samples measured in Gif (Figure S1).

[e]We considered a sea level drop of 50 m and 60 m for MIS 5.5–5.4 and MIS 5.1–4 transitions, respectively [*Waelbroeck et al.*, 2002], i.e., an ice volume correction of 0.40‰ and 0.48‰, respectively (considering a δ^{18}O increase of 0.008 ± 0.002‰ per meter of global sea level drop [*Duplessy et al.*, 2007]).

[f]Corresponding temperature amplitudes were calculated by considering that the ice volume–corrected δ^{18}O data only depend on temperature changes and using a coefficient of 1/4.38‰ °C^{-1} [*Shackleton*, 1974].

[g]The surface water cooling here exceeds the ice volume–corrected amplitude of planktic δ^{18}O variations: this suggests that freshening of surface waters compensates in part the effect of cooling on foraminiferal δ^{18}O.

study) to the deuterium record of EPICA Dome C (EDC) ice core [*EPICA Community Members*, 2004] placed on its most recent time scale EDC3 [*Parrenin et al.*, 2007]. Ages between the tie points are calculated by a simple linear interpolation (Analyseries software) [*Paillard et al.*, 1996].

[20] Core MD02-2488 established chronology implies a relatively high sedimentation rate over MIS 6 to 4 (Figure S2) (in average 14.6 cm/ka for the period 140–50 ka), with higher sedimentation rates during colder periods and lower sedimentation rates during the warm substages.[1] This is consistent with the main productivity areas located close to MD02-2488 site during cold periods, and further south during warmer intervals. The 2σ chronological uncertainty over the period 140–50 ka varies between 0.2 ka and 1.0 ka (on average 0.4 ka) for core MD02-2488 relatively to EPICA Dome C, and between 0.5 ka and 1.2 ka (on average 0.6 ka) for cores MD97-2120 and ODP 1089 relatively to core MD02-2488 (Figure S3).

[21] Cores MD94-101, MD94-102, MD00-2374 and MD88-770 (Figure 1b), which are all presently bathed by the same Circumpolar Deep Waters, were transferred on the Southern Ocean chronology by tying their benthic δ^{18}O records to that of core MD02-2488. The 2σ uncertainties of their chronology relatively to core MD02-2488 vary between 0.1 ka and 1.9 ka (Figure S3).

[22] Similarly, the age model of the South Atlantic core MD02-2589 is defined (following *Molyneux et al.* [2007]) by benthic synchronization to core MD97-2120 (on EDC3 time scale): hence, the South Atlantic benthic δ^{18}O variations are also consistent with those recorded in the South Indian core MD02-2488.

[23] The interhemispheric chronostratigraphy used in the present study is also based on benthic foraminifera δ^{18}O correlations: the two North Atlantic cores SU90-08 and CH69-K09 are located deeper than 3000 m water depth, as the Southern Ocean core MD02-2488. Temporal differences in the benthic δ^{18}O records are essentially observed between intermediate and deep water changes, and smaller within deep water variations [*Labeyrie et al.*, 2005].

3. Results

[24] Stages and substages are well marked in all records (Figure 5), with small but significant suborbital variability observed throughout the 130–60 ka interval. Here, our study is focused on the two phases of major variations over the last glacial inception: the MIS 5.5–5.4 (125–105 ka) and the MIS 5.1–4 (85–65 ka) transitions. During both periods, a large temperature drop is recorded in subantarctic surface waters (Figure 5b and Table 2). Simultaneously, planktic δ^{18}O data indicate major surface water changes (Figure 5c): the SST decrease here exceeds the ice volume–corrected amplitude of planktic δ^{18}O variations (Table 2). This suggests that freshening of surface waters compensates in part the effect of cooling on foraminiferal δ^{18}O.

[25] Major benthic δ^{18}O variations are also observed during both transitions (Figure 5d). Here again, the amplitude of benthic δ^{18}O increase exceeds the mean ocean δ^{18}O change because of the growth of Northern Hemisphere ice sheets and corresponding sea level drop [*Waelbroeck et al.*, 2002] (Table 2). Thus hydrological changes, i.e., intermediate and deep water cooling (and local changes in salinity), occurred in the Southern Ocean during these transitions.

[26] Besides, intermediate waters are characterized by high δ^{13}C values throughout MIS 5, with limited changes at substage boundaries and a larger δ^{13}C shift (of 0.5‰, Table 2) at the MIS 5.1–4 transition (Figure 5e). This rapid δ^{13}C shift (lasting less than 1 ka) is also recorded in the South Atlantic core MD02-2589 [*Molyneux et al.*, 2007] (Table 1 and Figure 6).

[1]Auxiliary materials are available in the HTML. doi:10.1029/2008PA001603.

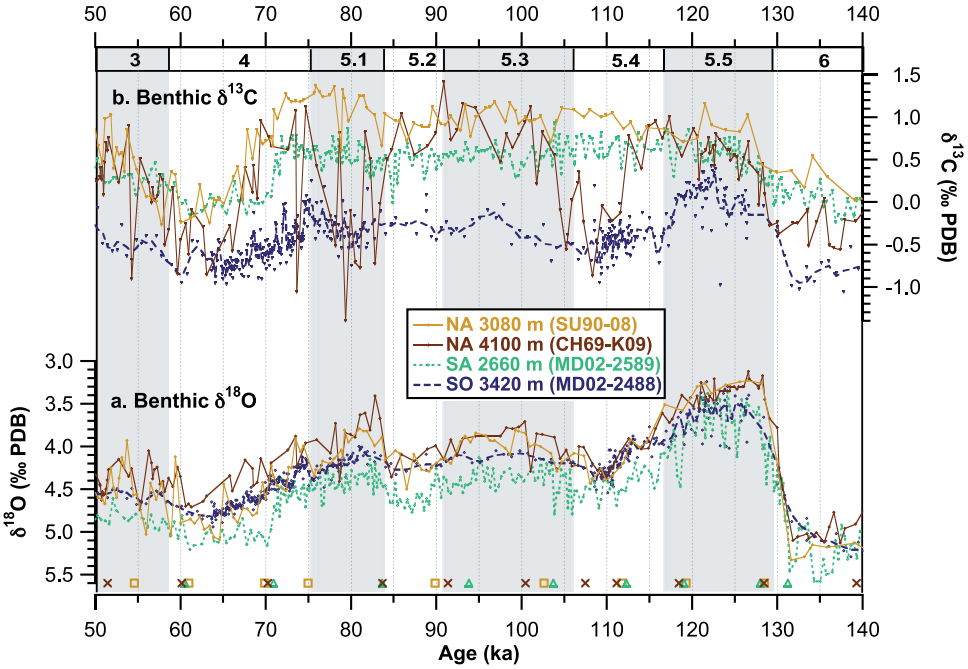

Figure 6. (a) Benthic δ^{18}O and (b) *Cibicides* δ^{13}C data from the North Atlantic (NA) cores SU90-08 (3080 m, light brown line) [*Cortijo*, 1995; *Grousset et al.*, 1993] and CH69-K09 (4100 m, dark brown line) [*Cortijo*, 1995; *Labeyrie et al.*, 1999] and the South Atlantic (SA) core MD02-2589 (2660 m, green dotted line) [*Molyneux et al.*, 2007], in comparison with the Southern Ocean (SO) core MD02-2488 (3420 m, dark blue dashed curves) (this study). The age models of the North and South Atlantic cores have been defined by benthic δ^{18}O synchronization (see text). No smoothing is applied in the North and South Atlantic records. Tie points for cores SU90-08 (light brown squares), CH69-K09 (dark brown crosses), and MD02-2589 (green triangles) are indicated at the bottom. The marine isotope stages are indicated at the top, with the warm substages highlighted by the gray-shaded areas.

[27] On the contrary, δ^{13}C records from the two deeper cores show, in addition to substages oscillations, the two large shifts seen in δ^{18}O records (Figure 5e). The first δ^{13}C shift ($\Delta\delta^{13}$C of -0.5‰ at 3400 m and -0.4‰ at 4600 m, Table 2) occurred at midtransition of the benthic δ^{18}O increase, while δ^{13}C values of intermediate waters remain high. The second δ^{13}C shift ($\Delta\delta^{13}$C of -0.4‰ at 3400 m and -0.7‰ at 4600 m, Table 2) took place over about 10 ka, at about the same period as the single δ^{13}C shift recorded at intermediate depths. Moreover, in cores MD02-2488 and ODP 1089, similar δ^{13}C values are recorded over the period 140–50 ka (Figure 5e); this suggests that both sites were bathed by close water masses.

[28] Both δ^{13}C shifts are likely to integrate at least part of the mean global ocean $\Delta\delta^{13}$C ≈ -0.4‰ change between interglacial and peak glacial [*Curry et al.*, 1988; *Michel et al.*, 1995]. However, we can reasonably consider that the global δ^{13}C changes did not exceed that value for each of these transitions. As the recorded δ^{13}C changes are larger, a reduction of ventilation is therefore observed in the deep and intermediate Southern Ocean during the last glacial inception.

4. Discussion

4.1. Assessing the Influence of NADW Changes

[29] We first investigated the mechanisms which could explain the reduction of ventilation observed in deep waters at the MIS 5.5–5.4 transition, whereas the ventilation of intermediate waters is not affected. Because Circumpolar Deep Waters form by mixing of NADW and recirculated deep waters from the Pacific and Indian oceans, both changes in NADW carbon isotope composition or in the relative proportion of NADW would affect the carbon isotope composition of CDW. To assess the influence of NADW ventilation changes on southern deep waters, we compare the Southern Ocean record of core MD02-2488 with three cores from the North and South Atlantic (Figure 6).

[30] The *Cibicides* record from the shallowest North Atlantic core SU90-08 (43°N, 30°W, 3080 m) [*Cortijo*, 1995; *Grousset et al.*, 1993] show high δ^{13}C values between 125 and 75 ka (Figure 6b). This indicates the presence of well-ventilated NADW at 3000 m in the western North Atlantic throughout MIS 5. The same δ^{13}C pattern is observed in several cores collected above 3000 m in the eastern and western basins of the North Atlantic (e.g., in cores SU90-38 (54°N, 21°W, 2900 m) [*Cortijo*, 1995], SU90-03 (40°N, 32°W, 2475 m) [*Chapman and Shackleton*, 1998], ODP 1057 (32°N, 76°W, 2584 m) [*Evans et al.*, 2007] and ODP 1059 (32°N, 75°W, 2985 m) [*Evans et al.*, 2007]). Therefore, North Atlantic Deep Waters ventilation did not change significantly before the beginning of the glacial period (MIS 4).

[31] In a few North Atlantic cores collected around 3200 m (e.g., cores MD95-2042 (38°N, 10°W, 3150 m) [*Shackleton et al.*, 2000, 2002, 2003], and NEAP18K (52.7°N, 30.3°W, 3275 m) [*Chapman and Shackleton*, 1999]), a slight $\delta^{13}C$ decrease (of around 0.2‰) is observed at the beginning of the MIS 5.5–5.4 transition. This suggests a limited shoaling of NADW lower boundary; it is however unlikely to cause the large $\delta^{13}C$ shift recorded in the deep Southern Ocean.

[32] Indeed, in the South Atlantic, the *Cibicides* record from core MD02-2589 (41.5°S, 25°E, 2660 m) [*Molyneux et al.*, 2007]) also shows high $\delta^{13}C$ values throughout MIS 5 (Figure 6b). This indicates that, during the entire stage 5, a well-ventilated NADW was reaching the South Atlantic, at least above 3000 m, and entering the Southern Ocean, before mixing with Pacific/Indian deep waters.

[33] Furthermore, in the North Atlantic, benthic records from cores collected deeper than 3000 m (e.g., cores MD95-2042 (38°N, 10°W, 3150 m) [*Shackleton et al.*, 2000, 2002, 2003], NEAP18K (52.7°N, 30.3°W, 3275 m) [*Chapman and Shackleton*, 1999] and CH69-K09 (42°N, 47°W, 4100 m) [*Cortijo*, 1995; *Labeyrie et al.*, 1999]) show during each substage, $\delta^{13}C$ modulations whose amplitude increases with the core water depth. These $\delta^{13}C$ shifts have been interpreted as an increased influence of poorly ventilated AABW in the deep North Atlantic and shoaling of NADW. This is supported by $\delta^{13}C$ values in the deeper core CH69-K09, which approach those recorded in the deep South Indian core at each $\delta^{13}C$ shift (Figure 6b). However, at the MIS 5.5–5.4 transition, the $\delta^{13}C$ shift observed in the deep North Atlantic (as illustrated by core CH69-K09 in Figure 6b) occurred when benthic $\delta^{18}O$ values were almost maximal, i.e., several thousands years after the $\delta^{13}C$ drop recorded in southern deep waters.

[34] In conclusion, the $\delta^{13}C$ drop observed in the Southern Ocean at the MIS 5.5–5.4 transition occurred several thousands years before any significant deep water changes in the North Atlantic: its origin has to be looked for in the Southern Ocean rather than in the North Atlantic.

4.2. Evidence for Northward Expansion of Poorly Ventilated Antarctic Bottom Water Mass During These Periods

[35] The spatial study of deep water changes in the Southern Ocean may be described using four additional cores from the South Indian sector (Figure 1b and Table 1). The two large drops in the benthic $\delta^{13}C$ are also observed in the cores (Figure 7). Despite their low temporal resolution, the $\delta^{13}C$ shift recorded in both northern cores lag by around 4 ka the $\delta^{13}C$ shift observed in the southern cores (Figure 7b, light gray-shaded areas). This suggests a progressive northward expansion of the boundary of a poorly ventilated water mass, with low $\delta^{13}C$ values (likely equivalent to AABW), from the southern sites to the northern sites. Moreover, the northern sites, which show higher $\delta^{13}C$ values than in the southern cores throughout MIS 5 and 4 (Figure 7b), appear closer to the zone of transition (strong $\delta^{13}C$ gradient) between poorly ventilated AABW and better ventilated CDW.

[36] Besides, a larger SST decrease is observed in the southern cores (MD02-2488 and MD88-770) compared to the northern cores (MD94-101 and MD94-102) at both MIS 5.5–5.4 and MIS 5.1–4 transitions (Figure 7c). This suggests an equatorward shift of the oceanic surface fronts [*Howard and Prell*, 1992; *Labeyrie et al.*, 1996]. The subantarctic front may have experienced a more pronounced northward shift than the subtropical front. Or it could have shifted in between the northern and southern cores locations, thus inducing a steeper meridional SST gradient.

[37] Finally, the comparison of the timing of SST and benthic $\delta^{13}C$ shifts within each of the cores indicate that the maximum of deep water $\delta^{13}C$ shift occurred after the maximum of cooling in the subantarctic waters during both MIS 5.5–5.4 and MIS 5.1–4 transitions (Figure 7, dark gray-shaded areas). This indicates that the equatorward shift of oceanic surface fronts and the associated climate changes may have induced the progressive northward expansion of poorly ventilated AABW in the deep Southern Ocean.

4.3. Proposed Mechanisms: Ocean-Atmosphere Interactions

[38] In this section, we propose mechanisms which could explain the deep water changes observed in the Southern Ocean over the last glacial inception. We present conceptual schemes for three time slices (MIS 5.5, MIS 5.4 and MIS 4) to illustrate the Southern Ocean circulation changes (Figure 8).

4.3.1. MIS 5.5–5.4 Transition (125–105 ka)

[39] The oceanic circulation of the last Interglacial period (MIS 5.5) (Figure 8a) was similar to the modern one [*Duplessy et al.*, 2007; *Duplessy and Shackleton*, 1985; *Evans et al.*, 2007]. We suggest that the early cooling observed in the high southern latitudes cores during MIS 5.5 (Figures 5a and 5b) induced an equatorward shift of the westerlies and associated oceanic fronts (Antarctic divergence, polar and subantarctic fronts) [*Toggweiler et al.*, 2006]. Such link is suggested by several indicators: glacial simulations with an atmospheric model (equatorward shift of the westerlies of 7° for a 3K cooling) [*Williams and Bryan*, 2006], paleoclimatic reconstructions (e.g., shift of the westerlies from ~50°S presently to ~41°S during glacial times in South America [*Moreno et al.*, 1999]), and by modern observations (a poleward shift of the westerlies is observed over the last 40 years) [*Hurrell and van Loon*, 1994; *Shindell and Schmidt*, 2004].

[40] The position of the Antarctic divergence (delimited between the subpolar westerly and peri-Antarctic easterly wind belts) and its associated Ekman transport, control the amount of upwelled Circumpolar Deep Waters in the Southern Ocean [*Toggweiler et al.*, 2006]. During cold periods, both the westerlies and the Antarctic divergence would be located further north. The peri-Antarctic easterly wind belt is constrained by the topography of the Antarctic ice sheet, itself mostly constrained by the coastline. We may therefore reasonably consider that the northward shift may be more pronounced for the westerly wind belt, moving away from the Antarctic divergence. The associated Ekman transport, hence the upwelling of relatively warm deep waters, would be reduced [*Toggweiler et al.*, 2006]. Reduced heat brought to Antarctic coastal waters would favor ice shelves expansion and sea ice formation during winters [*Hellmer*, 2004]. A greater winter sea ice cover, which is

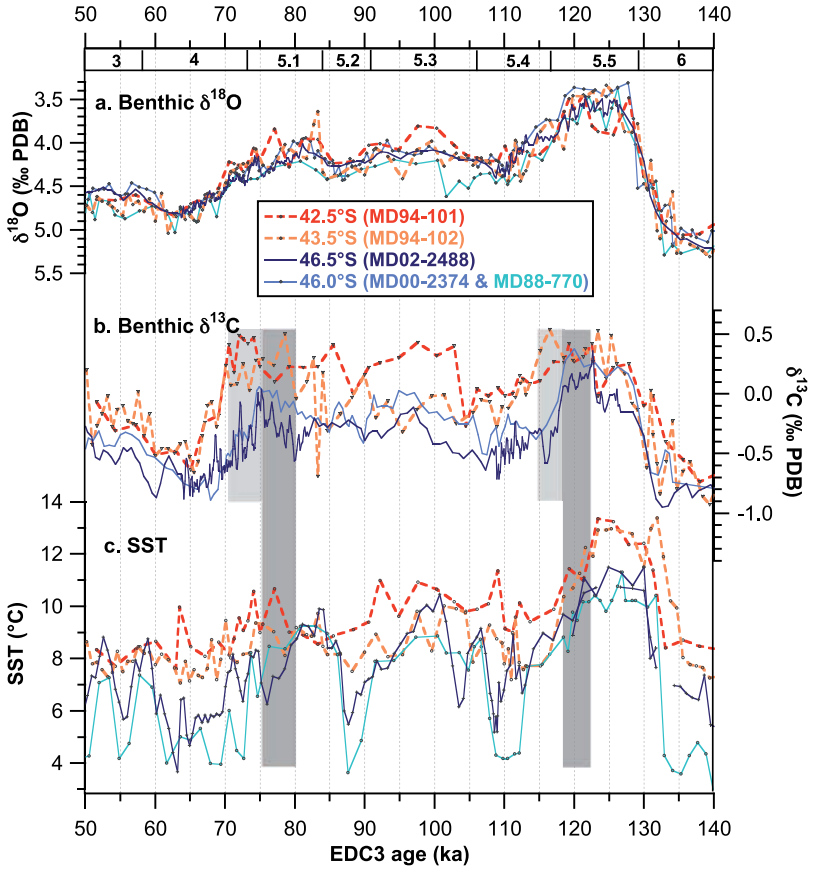

Figure 7. (a) Benthic δ^{18}O, (b) benthic δ^{13}C, and (c) SST data of cores MD94-101 (42.5°S, red dashed line) [*Lemoine*, 1998; *Salvignac*, 1998], MD94-102 (43.5°S, orange dashed line) [*Lemoine*, 1998; *Salvignac*, 1998], MD02-2488 (46.5°S, dark blue plain line) (this study), and MD88-770/MD00-2374 (46.0°S, light blue plain line) [*Duplessy et al.*, 2007; *Lemoine*, 1998; *Salvignac*, 1998] from the Indian sector of the Southern Ocean. A three-point moving average is presented only for the high-resolution benthic data of cores MD02-2488 and MD00-2374. The dark and light gray-shaded areas highlight the lead of surface water cooling over deep water δ^{13}C decrease and the lag of the δ^{13}C shift in the northernmost cores compared to the southernmost cores, respectively. The marine isotope stages are indicated at the top.

indeed observed during MIS 5.4 [*Bianchi and Gersonde*, 2002], would also be favored by the cooling in the high southern latitudes, as suggested by SST and Antarctic ice core records. Increased sea ice formation during winters would enhance the production of brine and deep convection of AABW [*Hellmer*, 2004].

[41] Enhanced production of cold AABW during colder climate would explain the increased contribution of AABW observed in the Southern Ocean and in the deep North Atlantic, and the deep water cooling recorded in the benthic δ^{18}O records of cores MD02-2488 and ODP 1089 during MIS 5.4 (Table 2). Besides, an increased sea ice cover around Antarctica during MIS 5.4 [*Bianchi and Gersonde*, 2002] would limit the air-sea gas exchanges in the polar surface waters and reduce the ventilation of AABW, as indicated by low benthic δ^{13}C values in the deep Southern Ocean (Figure 5e). In comparison, intermediate waters remained well ventilated (Figure 5e), but became colder (Table 2), probably because of a cooling in the subpolar waters, areas where these waters form.

[42] Therefore, the Southern Ocean circulation pattern during MIS 5.4 (Figure 8b), not so different from MIS 5.5 circulation (Figure 8a), is mostly characterized by an increased formation of poorly ventilated AABW, which expanded northward.

4.3.2. MIS 5.1–4 Transition (85–60 ka)

[43] The early cooling recorded in the high southern latitudes during MIS 5.1 (Figures 5a and 5b) induced the same sequence of ocean-atmosphere feedbacks in the Southern Ocean. Similar mechanisms would further enhance the formation of cold and poorly ventilated AABW, explain deep water changes observed in the Southern Ocean (i.e., deep water cooling and reduction of AABW ventilation, Table 2), and the northward propagation of AABW boundary in the Southern Ocean and the North Atlantic.

[44] Abrupt surface and intermediate water changes are observed in the Southern Ocean at the MIS 5.1–4 transition. Large planktic δ^{18}O increase and sea surface cooling, as recorded in core MD97-2120 (Figure 5 and Table 2), indicate a large northward shift of oceanic fronts in the southwestern

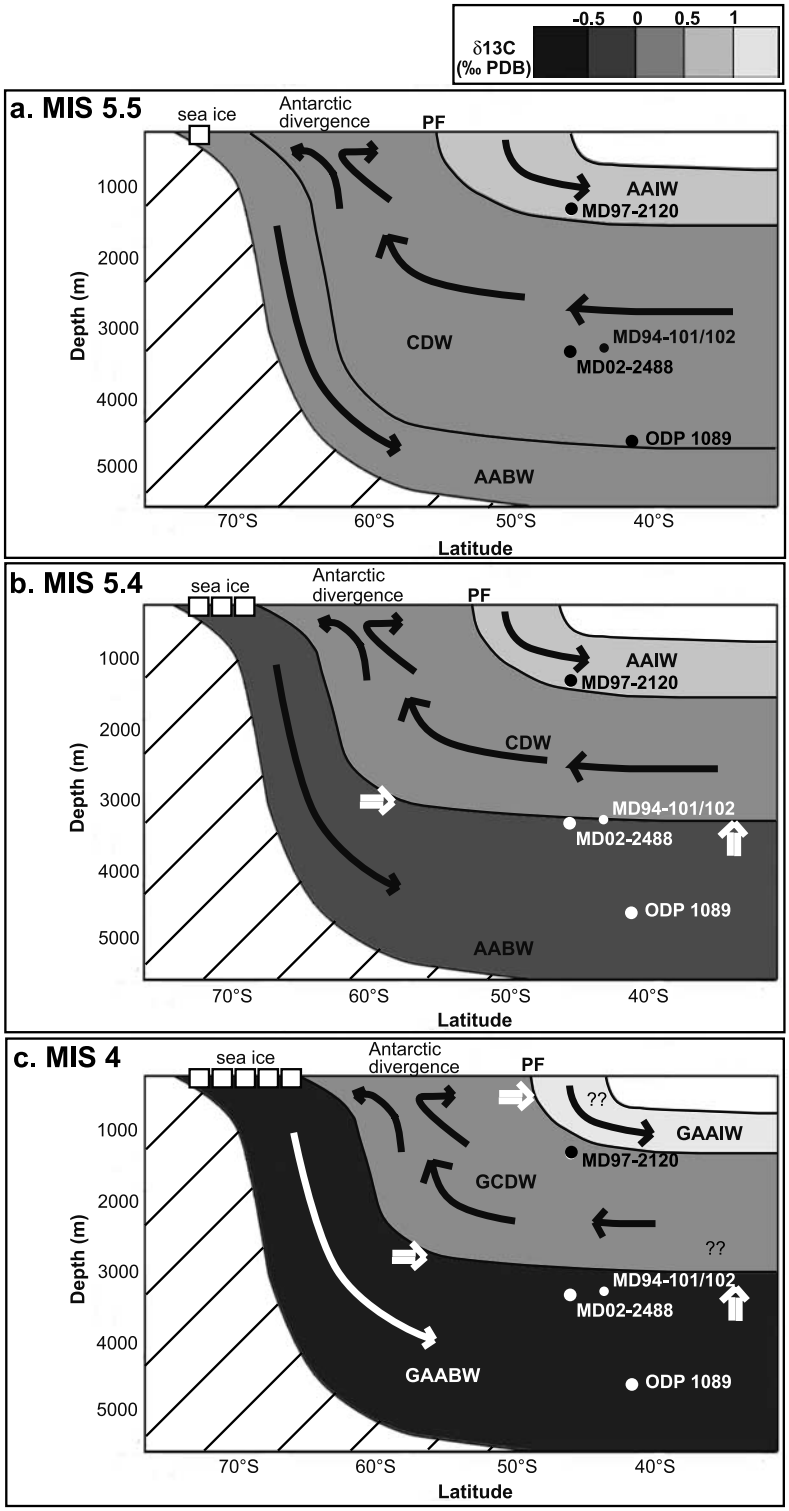

Figure 8. Conceptual schemes of the Southern Ocean circulation pattern proposed for (a) MIS 5.5, (b) MIS 5.4 to MIS 5.1, and (c) MIS 4. The locations of cores MD97-2120, MD02-2488, MD94-101/102, and ODP site 1089 are shown. The gray shading represents the degree of water mass ventilation in terms of $\delta^{13}C$ values. The main water masses are labeled: Antarctic Bottom Waters (AABW), Circumpolar Deep Waters (CDW), and Antarctic Intermediate Waters (AAIW). The letter "G" in the water masses name in Figure 8c indicates "glacial." "PF" refers to the polar front. The white double arrows highlight the northward expansion of AABW water mass and the northward shift of AAIW formation area.

Pacific (Figure 8c). Although core MD97-2120 remained north of the polar front, we propose that the intermediate water cooling and $\delta^{13}C$ decrease observed at that transition (Table 2) reflect a change of water mass at MD97-2120 site. Indeed, benthic $\delta^{13}C$ data from two shallow cores, KNR159-105JPC (27.3°S, 46.6°W, 1108 m) [*Curry and Oppo*, 2005] in the South Atlantic and MD06-2990 (42°19S 169°55E, 943 m) [*Steph et al.*, 2007] in the Tasman Sea, which are both presently lying in the core of AAIW, indicate a smaller $\delta^{13}C$ decrease (of around 0.3‰) at the MIS 5.1–4 transition. This $\delta^{13}C$ shift (maybe due to mean ocean $\delta^{13}C$ changes) indicates that AAIW remained well ventilated during MIS 4. Benthic $\delta^{13}C$ values from core MD97-2120, close to those of well ventilated AAIW at 943 m during interstadials [*Steph et al.*, 2007], deviate during glacials and approach the lower $\delta^{13}C$ values recorded at 1477 m in the same sector (core MD06-2986, 43°27S 167°54E, 1477 m) [*Steph et al.*, 2007]. Therefore, instead of lying in well-ventilated AAIW [*Pahnke and Zahn*, 2005], core MD97-2120 was bathed by less ventilated Circumpolar Deep Waters during MIS 4 (Figure 8c). This attests of a northward shift of the boundary between Antarctic Intermediate Water and Circumpolar Deep Water masses during MIS 4. It could possibly be associated with a reduction of AAIW formation in the south Pacific, as already proposed for the Last Glacial Maximum [*Bostock et al.*, 2004].

[45] Characterized by the expansion of poorly ventilated AABW and the northward shift of AAIW lower boundary, the deep circulation in the Southern Ocean during MIS 4 is already typical of glacial conditions [*Curry and Oppo*, 2005; *Duplessy et al.*, 1988].

5. Conclusions

[46] A comparison over the last glacial inception of three cores representing different Southern Ocean water masses suggests a decoupling between intermediate and deep water changes in the Southern Ocean. A large deep water $\delta^{13}C$ drop is observed during both periods of large surface cooling in the high southern latitudes (MIS 5.5–5.4 and MIS 5.1–4 transitions), whereas a major $\delta^{13}C$ decrease is recorded at intermediate depths at the MIS 5.1–4 transition only. A comparison with additional cores shows that the early southern deep water $\delta^{13}C$ drop occurred before any significant NADW ventilation changes in the North and South Atlantic: it reflects a reduction in AABW ventilation and a northward expansion of Antarctic Bottom Water mass in the deep Southern Ocean. We also show that these Southern Ocean deep water changes lag the cooling observed in subantarctic surface waters.

[47] We propose a succession of ocean-atmosphere feedbacks, in reaction to the early cooling observed in the high southern latitudes. Surface cooling at the MIS 5.5–5.4 transition would be associated with an equatorward shift of oceanic surface fronts and the westerlies, which moved away from the Antarctic divergence. The upwelling of Circumpolar Deep Waters would be reduced [*Toggweiler et al.*, 2006]. Both decreased heat brought to circumpolar surface waters and cooling in the high southern latitudes would enhance winter sea ice formation [*Hellmer*, 2004]. This would increase the related brine release and enhance deep convection of cold and poorly ventilated AABW.

[48] The Southern Ocean circulation of MIS 5.4 is mostly characterized by an increased formation of cold and poorly ventilated AABW, which expanded northward and reached shallower depths. During MIS 4, a further expansion of cold and poorly ventilated AABW and a northward shift in the boundary between AAIW and CDW suggest that the deep Southern Ocean circulation was already close to glacial conditions.

[49] **Acknowledgments.** Part of this study has been performed within the framework of the French National Research Agency ANR PICC project and of the European POP project (core MD00-2374 measurements). We thank Gulay Isguder and Loic Carlo for performing most of the foraminiferal counting on core MD02-2488. We also would like to acknowledge the crew of the research vessel *Marion-Dufresne* and the French Paul Emile Victor Institute (IPEV) (especially Yvon Balut) for collecting most of the cores studied here. Funding of the cruises has been facilitated by the IMAGES scientific program collaborations. This research also used samples and data provided by the Integrated Ocean Drilling Program (IODP). Finally, we would like to thank K. Pahnke and C. D. Charles for detailed and constructive reviews, which helped us to improve significantly the manuscript. This is LSCE contribution 3288.

References

Adkins, J. F., E. A. Boyle, L. D. Keigwin, and E. Cortijo (1997), Variability of the North Atlantic thermohaline circulation during the last interglacial period, *Nature*, *390*, 154–156, doi:10.1038/36540.

Barrows, T., S. Juggins, P. de Deckker, E. Calvo, and C. Pelejero (2007), Long-term sea surface temperature and climate change in the Australian–New Zealand region, *Paleoceanography*, *22*, PA2215, doi:10.1029/2006PA001328.

Bianchi, C., and R. Gersonde (2002), The Southern Ocean surface between marine isotope stages 6 and 5d: Shape and timing of climate changes, *Palaeogeogr. Palaeoclimatol. Palaeoecol.*, *187*, 151–177, doi:10.1016/S0031-0182(02)00516-3.

Bostock, H. C., B. N. Opdyke, M. K. Gagan, and L. K. Fifield (2004), Carbon isotope evidence for changes in Antarctic Intermediate Water circulation and ocean ventilation in the southwest Pacific during the last deglaciation, *Paleoceanography*, *19*, PA4013, doi:10.1029/2004PA001047.

Chapman, M. R., and N. J. Shackleton (1998), Millennial-scale fluctuations in North Atlantic heat flux during the last 150,000 years, *Earth Planet. Sci. Lett.*, *159*, 57–70, doi:10.1016/S0012-821X(98)00068-5.

Chapman, M. R., and N. J. Shackleton (1999), Global ice-volume fluctuations, North Atlantic ice-rafting events, and deep-ocean circulation changes between 130 and 70 ka, *Geology*, *27*, 795–798, doi:10.1130/0091-7613(1999)027<0795:GIVFNA>2.3.CO;2.

Cortese, G., A. Abelmann, and R. Gersonde (2007), The last five glacial-interglacial transitions: A high-resolution 450,000-year record from the subantarctic Atlantic, *Paleoceanography*, *22*, PA4203, doi:10.1029/2007PA001457.

Cortijo, E. (1995), La variabilité climatique rapide dans lAtlantique Nord depuis 128 000 ans: Relations entre les calottes de glace et locéan de surface, Ph.D. thesis, Univ. Paris XI, Orsay, France.

Cortijo, E., J. C. Duplessy, L. Labeyrie, H. Leclaire, J. Duprat, and T. C. E. van Weering (1994), Eemian cooling in the Norwegian Sea and North Atlantic ocean preceding continental ice-sheet growth, *Nature*, *372*, 446–449, doi:10.1038/372446a0.

Curry, W. B., and D. W. Oppo (2005), Glacial water mass geometry and the distribution of $\delta^{13}C$ of ΣCO_2 in the western Atlantic Ocean, *Paleoceanography*, *20*, PA1017, doi:10.1029/2004PA001021.

Curry, W. B., J. C. Duplessy, L. Labeyrie, and N. J. Shackleton (1988), Changes in the distribution of $\delta^{13}C$ of deep water ΣCO_2 between the last glaciation and the Holocene,

Paleoceanography, *3*, 317–341, doi:10.1029/PA003i003p00317.

Dezileau, L., G. Bareille, J. L. Reyss, and F. Lemoine (2000), Evidence for strong sediment redistribution by bottom currents along the southeast Indian ridge, *Deep Sea Res., Part I*, *47*, 1899–1936, doi:10.1016/S0967-0637(00)00008-X.

Duplessy, J. C. (1978), Isotope studies, in *Climatic Studies*, edited by J. Gribbin, pp. 46–67, Cambridge Univ. Press, Cambridge, U. K.

Duplessy, J. C., and N. J. Shackleton (1985), Response of global deep-water circulation to Earths climatic change 135,000–107,000 years ago, *Nature*, *316*, 500–507, doi:10.1038/316500a0.

Duplessy, J. C., N. J. Shackleton, R. G. Fairbanks, L. Labeyrie, D. W. Oppo, and N. Kallel (1988), Deepwater source variations during the last climatic cycle and their impact on the global deepwater circulation, *Paleoceanography*, *3*, 343–360, doi:10.1029/PA003i003p00343.

Duplessy, J. C., D. M. Roche, and M. Kageyama (2007), The deep ocean during the last interglacial period, *Science*, *316*, 89–91, doi:10.1126/science.1138582.

EPICA Community Members (2004), Eight glacial cycles from an Antarctic ice core, *Nature*, *429*, 623–628, doi:10.1038/nature02599.

EPICA Community Members (2006), One-to-one coupling of glacial climate variability in Greenland and Antarctica, *Nature*, *444*, 195–198, doi:10.1038/nature05301.

Evans, H. K., I. R. Hall, G. G. Bianchi, and D. W. Oppo (2007), Intermediate water links to Deep Western Boundary Current variability in the subtropical NW Atlantic during marine isotope stages 5 and 4, *Paleoceanography*, *22*, PA3209, doi:10.1029/2006PA001409.

Grousset, F. E., L. Labeyrie, J. A. Sinko, M. Cremer, G. C. Bond, J. Duprat, E. Cortijo, and S. Huon (1993), Patterns of ice-rafted detritus in the glacial North Atlantic, *Paleoceanography*, *8*, 175–192, doi:10.1029/92PA02923.

Hellmer, H. H. (2004), Impact of Antarctic ice shelf basal melting on sea ice and deep ocean properties, *Geophys. Res. Lett.*, *31*, L10307, doi:10.1029/2004GL019506.

Hodell, D. A., C. D. Charles, J. H. Curtis, P. G. Mortyn, U. S. Ninnemann, and K. A. Venz (2002), Data report: Oxygen isotope stratigraphy of ODP Leg 177 sites 1088, 1089, 1090, 1093, and 1094, *Proc. Ocean Drill. Program Sci. Results*, *177*, 1–26.

Hodell, D. A., K. A. Venz, C. D. Charles, and U. S. Ninnemann (2003), Pleistocene vertical carbon isotope and carbonate gradients in the South Atlantic sector of the Southern Ocean, *Geochem. Geophys. Geosyst.*, *4*(1), 1004, doi:10.1029/2002GC000367.

Howard, W. R., and W. L. Prell (1992), Late Quaternary surface circulation of the Southern Indian Ocean and its relationship to orbital variations, *Paleoceanography*, *7*, 79–117, doi:10.1029/91PA02994.

Hurrell, J. W., and H. van Loon (1994), A modulation of the atmospheric annual cycle in the Southern Hemisphere, *Tellus, Ser. A*, *46*, 325–338, doi:10.1034/j.1600-0870.1994.t01-1-00007.x.

Kroopnick, P. M. (1985), The distribution of ^{13}C of ΣCO_2 in the world oceans, *Deep Sea Res., Part A*, *32*, 57–84, doi:10.1016/0198-0149(85)90017-2.

Kucera, M., et al. (2005), Reconstruction of sea-surface temperatures from assemblages of planktonic foraminifera: Multi-technique approach based on geographically constrained calibration data sets and its application to glacial Atlantic and Pacific Oceans, *Quat. Sci. Rev.*, *24*, 951–998, doi:10.1016/j.quascirev.2004.07.014.

Labeyrie, L., and J. C. Duplessy (1985), Changes in the oceanic $^{13}C/^{12}C$ ratio during the last 140000 years: High-latitude surface water records, *Palaeogeogr. Palaeoclimatol. Palaeoecol.*, *50*, 217–240.

Labeyrie, L., J. C. Duplessy, and P. L. Blanc (1987), Variations in mode of formation and temperature of oceanic deep waters over the past 125,000 years, *Nature*, *327*, 477–482, doi:10.1038/327477a0.

Labeyrie, L., et al. (1996), Hydrographic changes of the Southern Ocean (southeast Indian sector) over the last 230 kyr, *Paleoceanography*, *11*, 57–76, doi:10.1029/95PA02255.

Labeyrie, L., H. Leclaire, C. Waelbroeck, E. Cortijo, J. C. Duplessy, L. Vidal, M. Elliot, and B. Le Coat (1999), Temporal variability of the surface and deep waters of the north west Atlantic Ocean at orbital and millennial scales, in *Mechanisms of Global Climate Change at Millennial Time Scales*, *Geophys. Monogr. Ser.*, vol. 112, edited by P. U. Clark, R. S. Webb, and L. D. Keigwin, pp. 77–98, AGU, Washington, D. C.

Labeyrie, L., C. Waelbroeck, E. Cortijo, E. Michel, and J. C. Duplessy (2005), Changes in deep water hydrology during the last deglaciation, *C.R. Geosci.*, *337*, 919–927, doi:10.1016/j.crte.2005.05.010.

Lemoine, F. (1998), Changements de lhydrologie de surface (température et salinité) de locéan Austral en relation avec les variations de la circulation thermohaline au cours des deux derniers cycles climatiques, thesis, Univ. Paris VI, Paris.

Levitus, S., and T. P. Boyer (1994), *World Ocean Atlas 1994*, vol. 4, *Temperature, NOAA Atlas NESDIS*, vol. 4, 129 pp., NOAA, Silver Spring, Md.

Lynch-Stieglitz, J., T. Stocker, W. Broecker, and R. G. Fairbanks (1995), The influence of air-sea exchange on the isotopic composition of oceanic carbon: Observations and modeling, *Global Biogeochem. Cycles*, *9*, 653–665, doi:10.1029/95GB02574.

Mackensen, A., D. K. Fütterer, H. Grobe, and G. Schmiedl (1993), Benthic foraminiferal assemblages from the eastern South Atlantic Polar Front region between 35° and 57°S: Distribution, ecology and fossilization potential, *Mar. Micropaleontol.*, *22*, 33–69, doi:10.1016/0377-8398(93)90003-G.

Mackensen, A., M. Rudolph, and G. Kuhn (2001), Late Pleistocene deep-water circulation in the subantarctic eastern Atlantic, *Global Planet. Change*, *30*, 197–229, doi:10.1016/S0921-8181(01)00102-3.

Mazaud, A., C. Kissel, C. Laj, M. A. Sicre, E. Michel, and J. L. Turon (2007), Variations of the ACC-CDW during MIS3 traced by magnetic grain deposition in midlatitude South Indian Ocean cores: Connections with the Northern Hemisphere and with central Antarctica, *Geochem. Geophys. Geosyst.*, *8*, Q05012, doi:10.1029/2006GC001532.

McManus, J. F., G. C. Bond, W. Broecker, S. Johnsen, L. Labeyrie, and S. Higgins (1994), High-resolution climate records from the North Atlantic during the last interglacial, *Nature*, *371*, 326–329, doi:10.1038/371326a0.

Meredith, M. P., K. E. Grose, E. L. McDonagh, K. J. Heywood, R. D. Frew, and P. F. Dennis (1999), Distribution of oxygen isotopes in the water masses of Drake Passage and the South Atlantic, *J. Geophys. Res.*, *104*(C9), 20,949–20,962.

Michel, E., L. Labeyrie, J. C. Duplessy, N. Gorfti, M. Labracherie, and J. L. Turon (1995), Could deep Subantarctic convection feed the world deep basins during the last glacial maximum?, *Paleoceanography*, *10*, 927–942, doi:10.1029/95PA00978.

Molyneux, E. G., I. R. Hall, R. Zahn, and P. Diz (2007), Deep water variability on the southern Agulhas Plateau: Interhemispheric links over the past 170 ka, *Paleoceanography*, *22*, PA4209, doi:10.1029/2006PA001407.

Moreno, P. I., T. V. Lowell, G. L. Jacobson, and G. H. Denton (1999), Abrupt vegetation and climate changes during the Last Glacial Maximum and last termination in the Chilean Lake District: A case study from Canal de la Puntilla (41°S), *Geogr. Ann., Ser. A*, *81*, 285–311, doi:10.1111/j.0435-3676.1999.00059.x.

Mortyn, P. G., C. D. Charles, U. S. Ninnemann, K. Ludwig, and D. A. Hodell (2003), Deep sea sedimentary analogs for the Vostok ice core, *Geochem. Geophys. Geosyst.*, *4*(8), 8405, doi:10.1029/2002GC000475.

Ninnemann, U. S. (1999), Origin of global millennial scale climate events: Constraints from the Southern Ocean deep sea sedimentary record, in *Mechanisms of Global Change at Millennial Time Scales*, *Geophys. Monogr. Ser.*, vol. 112, edited by P. U. Clark, R. S. Webb, and L. D. Keigwin, pp. 99–112, AGU, Washington, D. C.

Olbers, D., V. V. Gouretski, G. Seiss, and J. Schröter (1992), *Hydrographic Atlas of the Southern Ocean*, Alfred Wegener Inst. for Polar and Mar. Res., Bremerhaven, Germany.

Ostermann, D. R., and W. B. Curry (2000), Calibration of stable isotopic data: An enriched $\delta^{18}O$ standard used for source gas mixing detection and correction, *Paleoceanography*, *15*, 353–360, doi:10.1029/1999PA000411.

Ostlund, H. G., H. Craig, W. S. Broecker, and D. Spenser (1987), GEOSECS Atlantic, Pacific and Indian Ocean expeditions: Shorebased data and graphics, *Rep. 7*, Natl. Sci. Found., Washington, D. C.

Pahnke, K., and R. Zahn (2005), Southern Hemisphere water mass conversion linked with North Atlantic climate variability, *Science*, *307*, 1741–1746, doi:10.1126/science.1102163.

Pahnke, K., R. Zahn, H. Elderfield, and M. Schulz (2003), 340,000-year centennial-scale marine record of Southern Hemisphere climatic oscillation, *Science*, *301*, 948–952, doi:10.1126/science.1084451.

Paillard, D., L. Labeyrie, and P. Yiou (1996), Macintosh program performs time-series analyses, *Eos Trans. AGU*, *77*(39), 379.

Parrenin, F., et al. (2007), The EDC3 chronology for the EPICA Dome C ice core, *Clim. Past*, *3*, 485–497.

Prell, W. L. (1985), The stability of low-latitude sea-surface temperatures: An evaluation of the CLIMAP reconstruction with emphasis on the positive SST anomalies, *Rep. TR025,* U. S. Dep. of Energy, Washington, D. C.

Salvignac, M. E. (1998), Variabilité hydrologiques et climatique de lOcéan Austral (secteur indien) au cours du Quaternaire terminal. Essai de corrélations inter-hémisphériques, thesis, Univ. Bordeaux I, Talence, France.

Schmidt, G. A., G. R. Bigg, and E. J. Rohling (1999), Global seawater oxygen-18 database, NASA Goddard Inst. for Space Stud., New

York. (Available at http://data.giss.nasa.gov/o18data/)

Schmitz, W. J. (1996), On the world ocean circulation, II, The Pacific and Indian oceans/a global update, report, Woods Hole Oceanogr. Inst., Woods Hole, Mass.

Shackleton, N. J. (1974), Attainment of isotopic equilibrium between ocean water and the benthonic foraminifera genus Uvigerina: Isotopic changes in the ocean during the last glacial, *Colloq. Int. CNRS*, *219*, 203–209.

Shackleton, N. J. (1977), Carbon-13 in Uvigerina: Tropical rainforest history and the equatorial Pacific carbonate dissolution cycles, in *The Fate of Fossil Fuel CO_2 in the Oceans*, edited by A. Malahoff, and N. R. Andersen, pp. 401–427, Plenum, New York.

Shackleton, N. J., M. A. Hall, and E. Vincent (2000), Phase relationships between millennial-scale events 64,000–24,000 years ago, *Paleoceanography*, *15*, 565–569, doi:10.1029/2000PA000513.

Shackleton, N. J., M. R. Chapman, M. F. Sanchez-Goni, D. Pailler, and Y. Lancelot (2002), The classic marine isotope substage 5e, *Quat. Res.*, *58*, 14–16, doi:10.1006/qres.2001.2312.

Shackleton, N. J., M. F. Sanchez-Goni, D. Pailler, and Y. Lancelot (2003), Marine isotope substage 5e and the Eemian Interglacial, *Global Planet. Change*, *36*, 151–155, doi:10.1016/S0921-8181 (02)00181-9.

Shindell, D. T., and G. A. Schmidt (2004), Southern Hemisphere climate response to ozone changes and greenhouse gas increases, *Geophys. Res. Lett.*, *31*, L18209, doi:10.1029/2004GL020724.

Skinner, L. C., and N. J. Shackleton (2003), Millennial-scale variability of deep-water temperature and $\delta^{18}O_{dw}$ indicating deep-water source variations in the Northeast Atlantic, 0–34 cal. ka BP, *Geochem. Geophys. Geosyst.*, *4*(12), 1098, doi:10.1029/2003GC000585.

Sowers, T., M. Bender, L. Labeyrie, D. Martinson, J. Jouzel, D. Raynaud, J. J. Pichon, and Y. S. Korotkevich (1993), A 135,000-year Vostok-Specmap common temporal framework, *Paleoceanography*, *8*, 737–766, doi:10.1029/93PA02328.

Steph, S., R. Tiedemann, A. Sturm, and D. Nürnberg (2007), Pleistocene changes in SW-Pacific intermediate water circulation, poster presented at 9th International Conference on Paleoceanography, Shanghai, China.

Theron, R., D. Paillard, E. Cortijo, J. A. Flores, M. Vaquero, F. J. Sierro, and C. Waelbroeck (2004), Rapid reconstruction of paleoenvironmental features using a new multiplatform program, *Micropaleontology*, *50*, 391–395.

Toggweiler, J. R., J. L. Russell, and S. R. Carson (2006), Midlatitude westerlies, atmospheric CO_2, and climate change during the ice ages, *Paleoceanography*, *21*, PA2005, doi:10.1029/2005PA001154.

Waelbroeck, C., J. Jouzel, L. Labeyrie, C. Lorius, M. Labracherie, M. Stievenard, and N. I. Barkov (1995), A comparison of the Vostok ice deuterium record and series from the Southern Ocean core MD88-770 over the last two glacial-interglacial cycles, *Clim. Dyn.*, *12*, 113–123, doi:10.1007/BF00223724.

Waelbroeck, C., L. Labeyrie, E. Michel, J. C. Duplessy, J. F. McManus, K. Lambeck, E. Balbon, and M. Labracherie (2002), Sea-level and deep water temperature changes derived from benthic foraminifera isotopic records, *Quat. Sci. Rev.*, *21*, 295–305, doi:10.1016/S0277-3791(01)00101-9.

Williams, G. P., and K. Bryan (2006), Ice age winds: An aquaplanet model, *J. Clim.*, *19*, 1706–1715, doi:10.1175/JCLI3766.1.

F. Dewilde, A. Govin, L. Labeyrie, E. Michel, and C. Waelbroeck, LSCE, IPSL, CEA, UVSQ, CNRS, F-91190 Gif sur Yvette, France. (aline.govin@lsce.ipsl.fr)

E. Jansen, Bjerknes Centre for Climate Research, University of Bergen, N-5007 Bergen, Norway.